ATOMIC NUCLEI AT HIGH EXCITATION ENERGY STUDIED WITH GIANT RESONANCES.

J. J. Gaardhøje, A. Maj[1], T. Tveter[2], Z. Zelazny
Niels Bohr Institute
Blegdamsvej 15-17, 2100 Copenhagen.
Denmark

F. Camera, A. Bracco, B. Million, M. Pignanelli
Dipartimento di Fisica, Universitá di Milano e INFN
Via Celoria 16, Milano, Italy

1. INTRODUCTION.

During the last few years the study of highly excited atomic nuclei through the investigation of collective vibrations of the neutrons and protons (giant dipole resonances -GDR) in such nuclei has developped considerably, experimentally as well as theoretically.

The experimental method relies on the measurement of the spectral and angular distribution of the high energy photons emitted when GDR's in hot nuclei are damped. Excited state GDR gamma ray spectroscopy has now established itself as the principal method to study the entire phase space available to the decay of a compound nucleus.

There are three regions in this space, spanned by the variables excitation energy E*, and angular momentum I (and mass number A), which are currently being explored vigourously. They are apparent from figure 1.

At the lowest excitation energies (low in this context) from E*=30Mev to E*=100 MeV, the study of the shapes of excited nuclei and the fluctuations of the shape provides a unique tool to follow the gradual disappearance of quantum effects in finite size quantum systems as the temperature increases. At higher energies, ranging up to excitation energies not far from the fragmentation limit (E*=500-1000 MeV), the study of the GDR gamma ray decay provides new information on the damping of collective excitations in hot nuclear matter and on the timescales associated with different types of nuclear motion. In very heavy nuclei or in nuclei which are rotating very fast and which thus are fission-unstable, the pre-fission GDR emission is also a new and powerful tool to study the properties of exotic nuclei under extreme conditions.

Here we discuss some of the phenomena which are observed in the two first mentioned regions and which provide new and basic information on the timescales associated with the hot compound nucleus. For recent reviews on GDR spectroscopy we refer reader to refs.[3] and [4] in which extensive reference lists may also be found. Since this is a school we take the opportunity to present in some detail the formalism underlying the data analysis. We hope that the interested reader will find this useful.

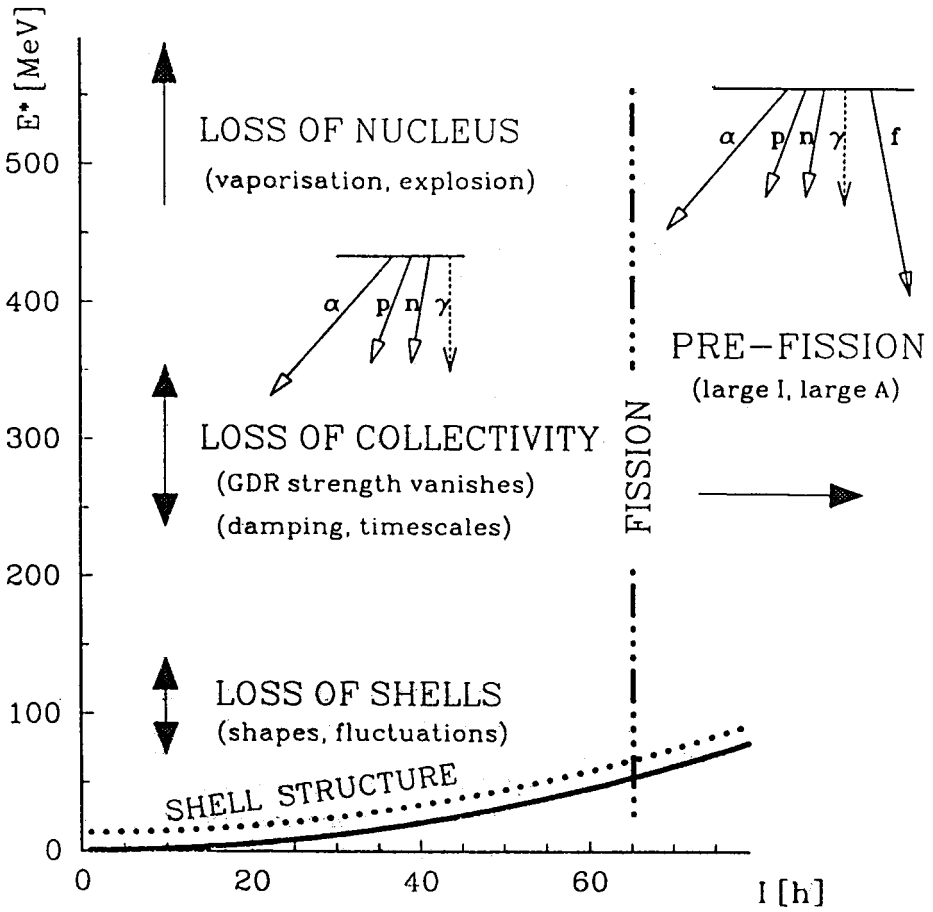

Figure 1: Schematic illustration of the phase space available to the decay of a hot and rotating compound nucleus. Indicated are the regions which are currently under investigation using excited-state GDR spectroscopy.

2. SOME BASIC CONCEPTS.

2.1 Statistical decay

Figure 2 shows a typical gamma ray spectrum obtained from the reaction $^{40}Ar + ^{70}Ge$ at 420 MeV [5], leading to the formation of ^{110}Sn isotopes with excitation energies around E^*=250 MeV. In this experiment using the SARA accelerator in Grenoble, the fusion residues were explicitly identified in a couple of parallel plate avalanche detectors located at forward angles. Thus the shown gamma ray spectrum is associated with emission from a fused compound

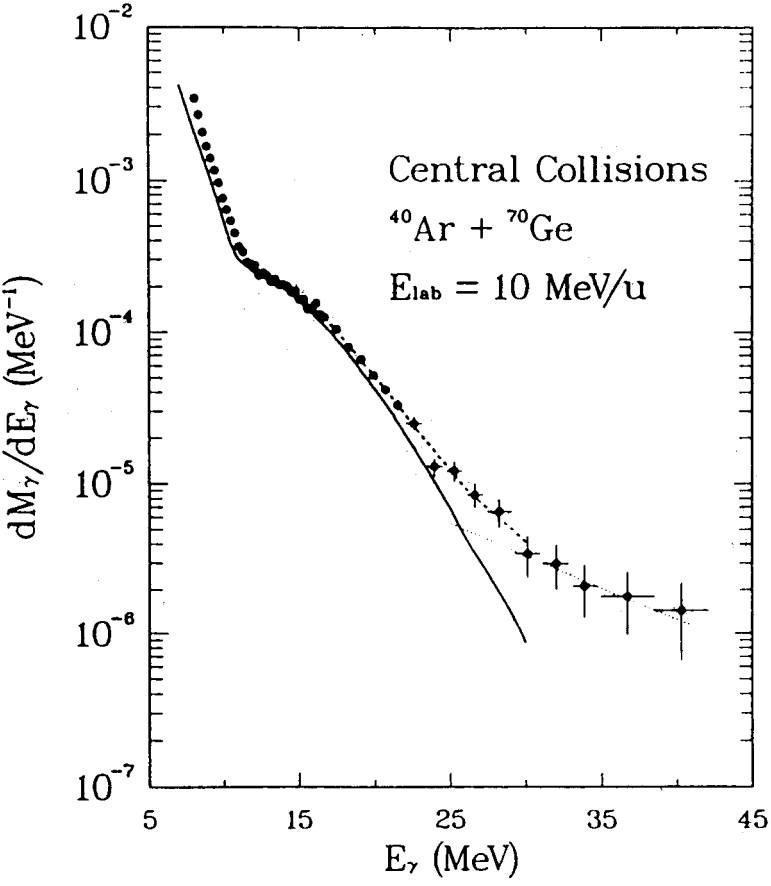

Figure 2: Spectrum of gamma rays from the reaction $^{40}Ar + ^{70}Ge$ in coincidence with detected residues from complete fusion.

system produced with rather well defined initial conditions (A and E^* are known). The lines are calculations which show the contribution from the nuclear decay (assumed to be statistical and originating from an equilibrated system) and from the nucleon-nucleon collisions that take place in the initial stages of the reaction in the course of the thermalisation proces. As far as the nuclear part is concerned it is composed of two pieces: at low gamma ray transition energies the spectrum consists almost exclusively of gamma rays emitted by the cold reaction residues, while in the energy range E_γ=10-25 MeV the emission is mainly associated with the decay of the GDR. That we indeed deal with a resonant process is apparent from figure 3 and 4, where the effect of the exponentially varying nuclear level density has been removed.

We see from figures 2, 3 and 4 (the latter is from ref. [6]) that the calculations are able to reproduce the measured spectra well. Indeed, until recently the basic tool for the analysis of gamma ray spectra from excited nuclei was the statistical model. We recall below some of its basic features.

In the statistical model for nuclear decay, the partial width for decay of a nucleus C into a system $A+a$, where a could stand for a particle or a gamma ray, can be written

$$\frac{d\Gamma_a}{dE_a} = \frac{(2I_a+1)k_a^2}{2\pi^2}\sigma(a+A\rightarrow C)\frac{\rho_A(E_A^*)}{\rho_C(E_C^*)} \qquad (1)$$

where ρ_C is the density of states at the excitation energy E^*_C of the compound nucleus, ρ_A is the density of states at the excitation energy of the daughter nucleus, k_a is the wave number of the relative motion of $A+a$ and I_a is the spin of fragment a. This expression is derived from Fermis's Golden rule for the formation of the compound nucleus in the process $a+A \rightarrow C$ and for the decay in the process $C \rightarrow A+a$, assuming detailed balance, i.e. that the matrix elements for both processes are identical. Thus the decay rate can be expressed in terms of the cross section for the inverse process of absorbtion, $\sigma(a+A \rightarrow C)$.

For gamma rays, $k_a = p/\hbar = E_\gamma/(\hbar c)$. The level densities, at a given spin and excitation energy, can be estimated[7] from the independent particle model, assuming an equal spacing of the nuclear levels

$$\rho(A,E,I) = \frac{2I+1}{12}\sqrt{a}\,(\frac{\hbar^2}{2J_{rig}})^{3/2}(E-\frac{\hbar^2 I(I+1)}{2J_{rig}})^{-2}\exp\{2\sqrt{a[E-\frac{\hbar^2}{2J_{rig}}I(I+1)]}\} \qquad (2)$$

Here a is the level density parameter, and J_{rig} the rigid body moment of inertia. In the Fermi gas model, a=A/15, while in finite size nuclei at lower temperature one may use a≈ A/8.

With such a level density formula, the partial decay width for gamma ray emission between two states of definite spin is

$$\frac{d\Gamma_\gamma}{dE_\gamma} = \frac{E_\gamma^2}{(\pi\hbar c)^2}\sigma_{abs}^{I_i\rightarrow I_f}(E_\gamma)\frac{\rho(E_f,I_f)}{\rho(E_i,I_i)} \approx \frac{E_\gamma^2}{(\pi\hbar c)^2}\frac{\sigma_{abs}(E_\gamma)}{3}\exp(-\frac{E_\gamma}{T}) \qquad (3)$$

For gamma ray emission in the GDR region one can use the absorbtion cross section, which is measured in photonuclear reactions on stable nuclei. The GDR line shape in cold nuclei can be well described by a Lorentzian function as expected for the scattering of gamma rays on a dipole oscillator. The same appears to be true for the photoexcitation of the plasmon resonance (the analog of the GDR for electronic systems) in excited metallic clusters of atoms.

Thus

$$\sigma_{abs}(E_\gamma) = \frac{\sigma_0\Gamma_{GDR}^2 E_\gamma^2}{(E_\gamma^2-E_{GDR}^2)^2+\Gamma_{GDR}^2 E_\gamma^2} \qquad (4)$$

where σ_0 is the strength, and E_{GDR} and Γ_{GDR} the centroid energy and width of the GDR, respectively.

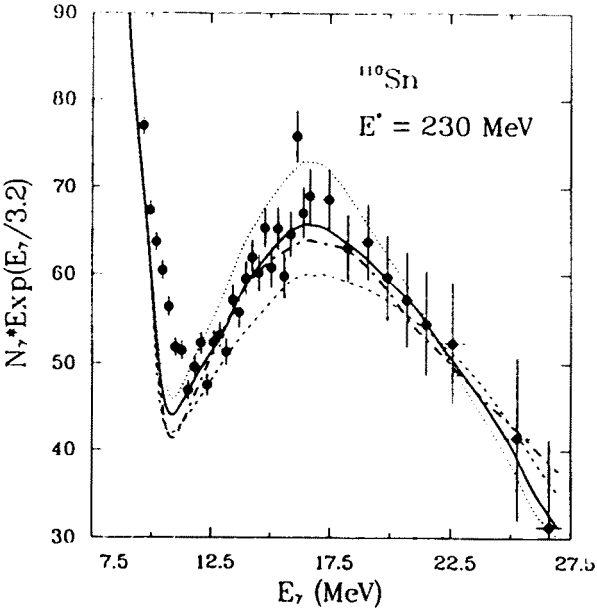

Figure 3: Photon spectrum from the decay of excited ^{110}Sn nuclei produced in the reaction ^{40}Ar + ^{70}Ge at 10 MeV/u.

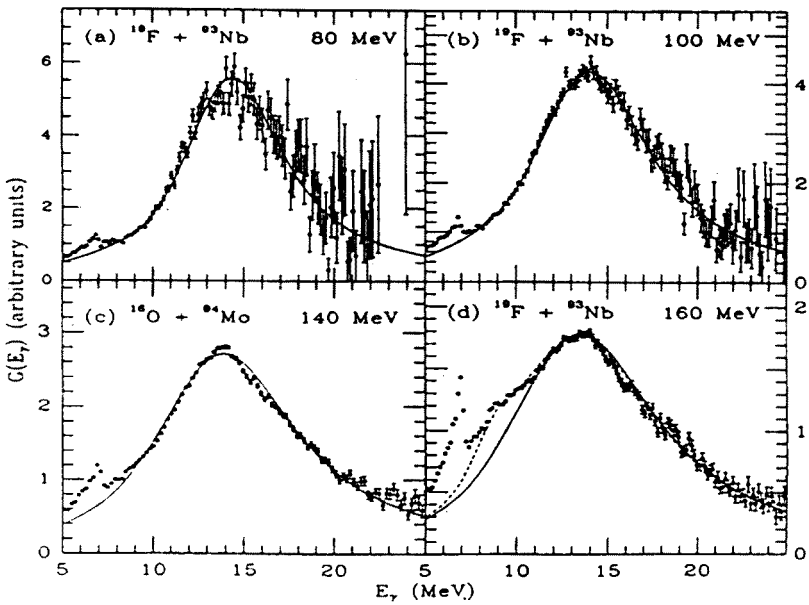

Figure 4: GDR gamma ray spectra from the decay of excited Sn nuclei at various excitation energies measured with the Stony Brook Tandem + Linac 2. The lines are statistical model calculations as described in the text.

The integral of the energy dependent absorbtion cross section over the energy range of the GDR can be expressed in terms of the Thomas-Reihe-Kuhn sum rule (the energy weighted sum rule) as follows

$$\begin{aligned}\int_0^{30}\sigma_{abs}(E_\gamma)\,dE_\gamma &= \frac{16\pi^3}{9\hbar c}\sum_a (E_f-E_0)\,B(E1,0\rightarrow f)\\ &= \frac{4\pi^2e^2\hbar}{2mc}\frac{NZ}{A}\\ &\approx 6\frac{NZ}{A}\ [MeV\,fm^2]\end{aligned} \tag{5}$$

Using that the area of a Lorentzian is

$$\int_0^{\infty}\frac{\sigma_0\Gamma_{GDR}^2E_\gamma^2}{(E_\gamma^2-E_{GDR}^2)^2+E_\gamma^2\Gamma_{GDR}^2}\,dE_\gamma = \frac{\pi\sigma_0\Gamma_{GDR}}{2} \tag{6}$$

the partial dipole gamma ray decay width can be written

$$\frac{d\Gamma_\gamma}{dE_\gamma} = \frac{4e^2}{3\pi mc\hbar^2c^2}\frac{NZ}{A}S_{GDR}\frac{\Gamma_{GDR}E_\gamma^4}{(E_\gamma^2-E_{GDR}^2)^2+\Gamma_{GDR}^2E_\gamma^2}\exp(-\frac{E_\gamma}{T}) \tag{7}$$

In the expression above the parameter S_{GDR} has been included as a scaling factor for the GDR strength in terms of the sum rule strength in connection with analyses of measured spectra.

It is interesting to note that equation 7 can also be derived, independently of assumptions about the ratio of the density of states, by considering the thermal radiation emitted by a hot nucleus, as pointed out by Brink[8] . The argument is based on a consideration of the nucleus in equilibrium with a heat bath of thermal radiation at temperature T.

The partial neutron decay width can be estimated from equation 1, yielding

$$\frac{d\Gamma_n}{dE_n} = \frac{(2I_n+1)k_n^2}{2\pi^2}\sigma_{abs}\frac{\rho_f(E^*-B_n-E_n)}{\rho_i(E^*)} \tag{8}$$

where E_n is the neutron kinetic energy and B_n is the binding energy of the neutron. With I_n= 1/2, k= p/ħ= $(2mE_n)/\hbar^2$, and assuming $\sigma_{abs}= \pi R^2$ one obtains

$$\frac{d\Gamma_n}{dE_n} = \frac{2mR^2}{\pi\hbar^2}E_n\exp(-\frac{B_n+E_n}{T}) \tag{9}$$

using again a level density expression as the one given in chapter 3, and assuming $B_n+E_n << E^*$.

The total neutron emission width, integrated over all neutron kinetic energies is then

$$\Gamma_n = \frac{2mR^2}{\pi\hbar^2} e^{-B_n/T} \int_0^\infty E_n e^{-E_n/T} dE_n$$
$$= \frac{2mr_0^2 A^{2/3}}{\pi\hbar^2} T^2 e^{-B_n/T} \qquad (10)$$

where we have used $R=r_0A^{1/3}$.

It is seen that the neutron decay probability increases with temperature. With this expression the typical evaporation times are $\tau_n \approx 3\times10^{-17}$s at T=1 MeV, $\tau_n \approx 3\times10^{-21}$s at T= 3 MeV, $\tau_n \approx 3\times10^{-22}$s at T= 5 MeV and $\tau_n \approx 1\times10^{-22}$s at T= 7 MeV, for nuclei in the A= 100 region.

These times should be compared to the typical GDR gamma ray emission probabilities, which can be estimated from the expressions given above. Considering again a nucleus with A≈ 100 and $E_{GDR} \approx$ 15 MeV the following lifetimes are obtained for a gamma ray with E_γ=15 MeV: $\tau_\gamma \approx 2\times10^{-13}$s at T=1 MeV, $\tau_\gamma \approx 8\times10^{-18}$s at T= 2 MeV and $\tau_\gamma \approx 1\times10^{-18}$s at T= 5 MeV and $\tau_\gamma \approx 5\times10^{-19}$s at T= 7 MeV. The slowness of the radiative decay of the GDR is the cause of the modest branching for gamma ray emission relative to that for particle emission, which is observed in experiment (≈10^{-4}).

A large number of reactions have now been studied by various groups and analyzed in a similar fashion using versions of the statistical model computer program CASCADE modified to include the gamma decay in competion with particle evaporation. The results of such analyses are shown in figure 5 and compared to the known data from ground state GDR's. The latter were extensively studied[9] by (γ,n) methods in the 1960-1970'es.

From the comparison between the data for cold and hot nuclei one can see that the general features of the GDR are very stable (strength in units of the classical sum rule and average resonance energy). The systematic variation of the GDR width seen in cold nuclei, which correlates with the nuclear magic numbers is however absent for hot nuclei. One finds systematically increased widths in hot nuclei.

For excited nuclei the data are however multidimensional and thus much richer than the corresponding T=0 MeV data. Figure 6 shows the generic view we now have of a giant resonance in hot nuclei, as exemplified by the systematics of the GDR parameters in Sn isotopes as a function of the excitation energy of the compound nucleus. We will come back to this figure repeatedly in the following discussion. In figure 7 we show another type of data cut: the centroid energy of the GDR plotted as a function of the angular momentum of the gamma ray emitting nucleus for various mass regions. It may be seen from figures 6 and 7 that the centroid energy of the GDR (and thus the nuclear volume and symmetry energy) does not depend significantly on the excitation energy and angular momentum of the decaying nucleus, in contrast to what was sometimes brought forward a few years ago.

The lowermost two rows in figure 5 display the nuclear elongation parameter β obtained from an analysis of GDR spectra using a double Lorentzian shape for the GDR strength function. The deformation is often calculated from the centroid energies of the two fitted components, $\beta = 1.05(d-1)d^{-1/3}$ with $E_b/E_a = 0.911d+0.089$ where *b* stands for the symmetry axis and *a* for the perpendicular axes. Also shown is the ratio of the extracted strengths in the two components, which for axially symmetric nuclei can be related to the shape (oblate or prolate). The described procedure implicitly assumes axially symmetric nuclei and is obviously of limited validity for nuclei with changing and fluctuating shapes. Nevertheless the data shown in figure 5 establishes the ocurrence of deformation in hot nuclei as a common phenomenon.

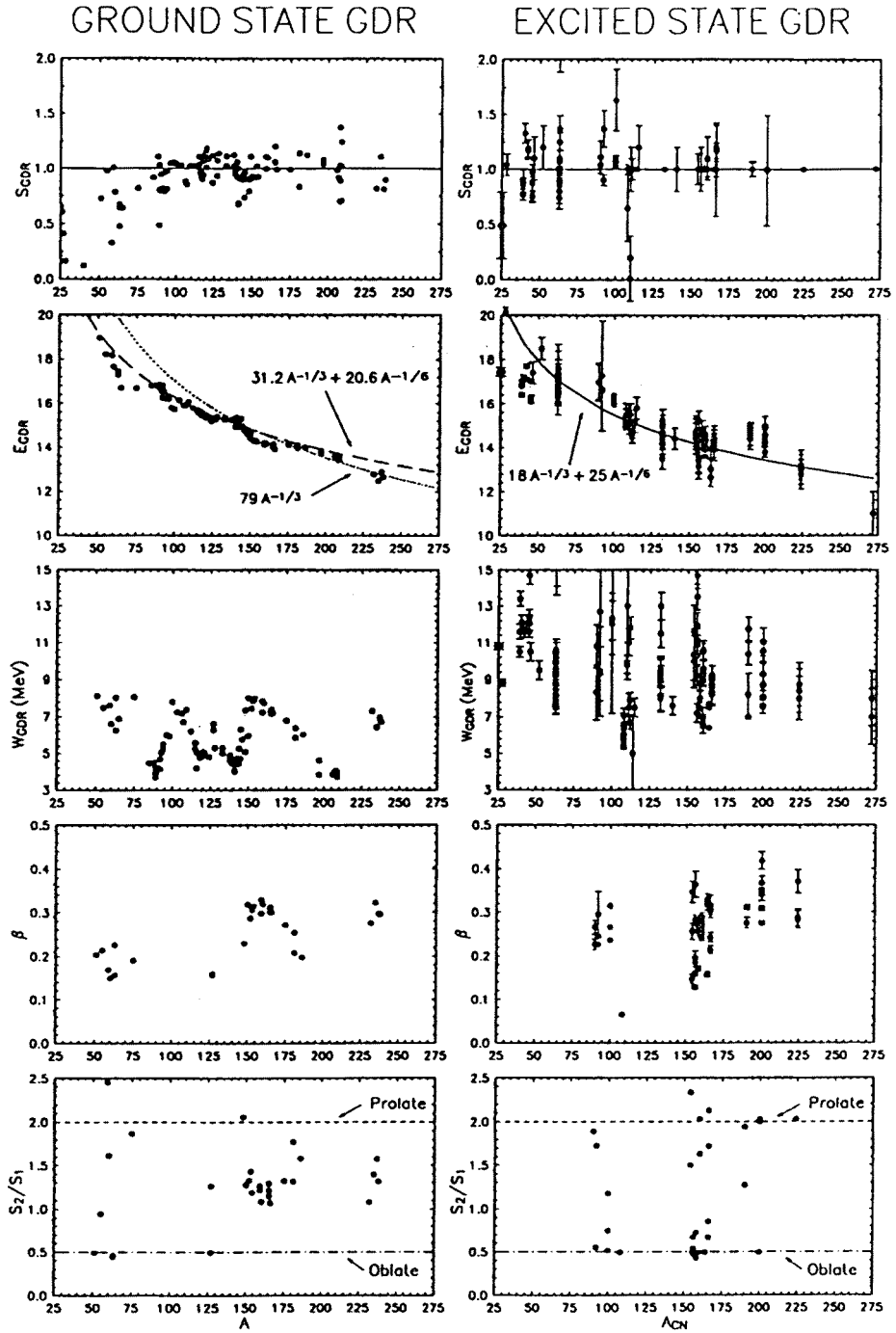

Figure 5: Systematic comparison of available data on giant dipole resonances in cold (left) and hot nuclei (right) as a function of the mass number. From top to bottom: strength, centroid..

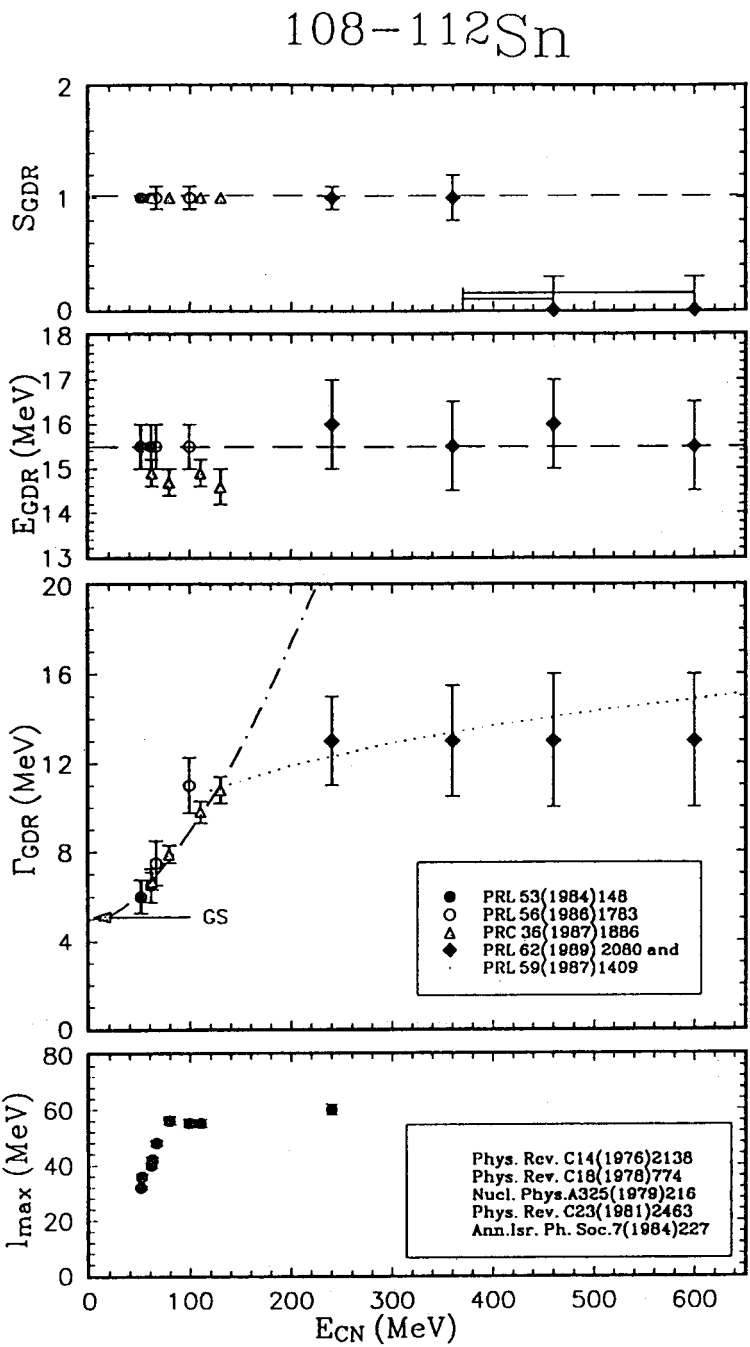

Figure 6: Systematics of GDR parameters (strength, centroid, width) as a function of the excitation energy of $^{108-112}$Sn isotopes. The bottom panel shows the maximum angular momentum of the compound nuclei surviving fission.

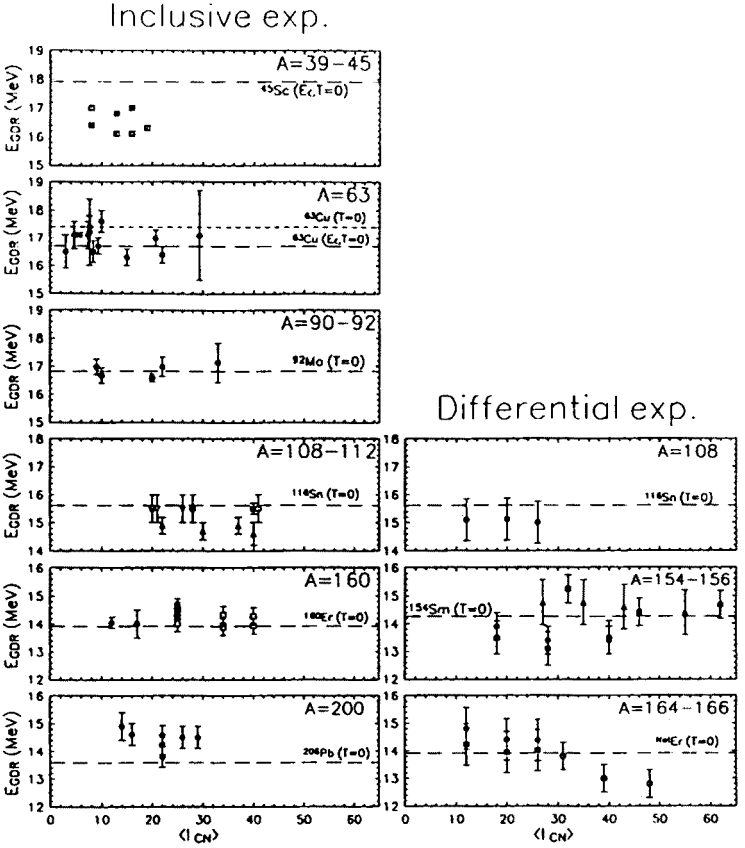

Figure 7: Systematics of the GDR centroid energy as a function of the angular momentum of the compound nucleus for different mass regions. Left: inclusive experiments, right: exclusive experiments with angular momentum gating.

2.2 The GDR in rotating nuclei.

For the purpose of simulating measured GDR distribution in hot and rotating nuclei from models it is convenient to keep in mind how we expect the GDR to behave in the general case of non-axial symmetric nuclei. This problem has been explored by many authors. In order to provide the reader with the possibility of doing such simulations with a simple program on his personal computer we list in the following the necessary expressions in a rather detailed fashion.

In non-rotating deformed nuclei the GDR splits up in vibrations with frequencies roughly inversely proportional to the length of the axes.

	Intrinsic frame		Laboratory frame		
i	Frequency	Strength	Mode	Frequency	Strength
1	ω_1	$\frac{1}{\omega_1}$	$\Delta I=0$	ω_1	$\frac{1}{\omega_1}$
2	Ω_2	$\frac{1}{\Omega_2}\frac{2\omega^2+\sqrt{D}}{\sqrt{D}}$	$\Delta I=+1$	$\Omega_2+\omega$	$\frac{1}{\Omega_2}\frac{(\Omega_2-\omega)^2-0.5(\omega_2^2+\omega_3^2)}{2\sqrt{D}}$
2			$\Delta I=-1$	$\Omega_2-\omega$	$\frac{1}{\Omega_2}\frac{(\Omega_2+\omega)^2-0.5(\omega_2^2+\omega_3^2)}{2\sqrt{D}}$
3	Ω_3	$\frac{1}{\Omega_3}\frac{-2\omega^2+\sqrt{D}}{\sqrt{D}}$	$\Delta I=+1$	$\Omega_3+\omega$	$\frac{1}{\Omega_3}\frac{-(\Omega_3-\omega)^2+0.5(\omega_2^2+\omega_3^2)}{2\sqrt{D}}$
3			$\Delta I=-1$	$\Omega_3-\omega$	$\frac{1}{\Omega_3}\frac{-(\Omega_3+\omega)^2+0.5(\omega_2^2+\omega_3^2)}{2\sqrt{D}}$

Table 1: Strenght and centroid energies of the GDR calculated in the harmonic oscillator model as described in the text.

The frequencies can be estimated from the Hill-Wheeler formula

$$\omega_k=\omega_{GDR}\exp[-\sqrt{\frac{5}{4\pi}}\beta\cos(\gamma-\frac{2\pi}{3}k)] \qquad (11)$$

where k= 1,2,3 labels the principal axes in the intrinsic frame and ω_{GDR} is the average frequency of the dipole vibration.

In the case of rotation the problem has been treated by many authors [10,11,12,13]. In general, Coriolis forces cause a further splitting of the components perpendicular to the rotation axis.

The eigenfrequencies in the intrinsic frame, obtained by solving the Hamiltonian

$$H=\frac{(\bar{p})^2}{2m}+V-\bar{\omega}\cdot(\bar{r}\times\bar{p}) \tag{12}$$

with a two dimensional oscillator potential V, are

$$\Omega_{2,3}^2=(\frac{\omega_2^2+\omega_3^2}{2})+\omega^2\pm\sqrt{D}$$

where

$$D=\frac{1}{4}(\omega_2^2-\omega_3^2)^2+2\omega^2(\omega_2^2+\omega_3^2) \tag{14}$$

In the laboratory frame, the eigenvalues are $\Omega_1=\omega_1$, $\Omega_{2,3}\pm\omega$. The associated strengths are listed in table 1. In the case of rotation around the symmetry axis, the frequencies in the laboratory frame are identical to the non-rotating frequencies.

2.3 The GDR angular distribution.

2.3.1 General concepts.

The measurement of the angular distribution of the GDR photons provides a complementary method to study the GDR in hot nuclei that are aligned in space due to rotation[14]. It has several advantages over the more standard analysis of the spectrum shape. Indeed, experimental angular distributions are to a large extent free from possible systematic errors originating from the statistical analysis of the spectrum, due in particular to assumptions about the nuclear level density at finite temperature. Furthermore, the angular distribution depends markedly on the *orientation* of the nucleus with respect to the direction of the total angular momentum vector, I_{tot}.

The angular distribution depends on whether a given vibration is along an axis parallel or perpendicular to the direction of I_{tot}. For example, in a prolate nucleus rotating collectively, I_{tot} is perpendicular to the symmetry axis. The angular momentum associated with the GDR component at lower energy, which corresponds to a vibration along the symmetry axis, is therefore parallel to I_{tot} and couples to I_{tot}. The associated transition is stretched ($|\Delta I|=1$). The two degenerate high energy GDR components, associated with vibrations along the short axes, that are parallel and perpendicular to I_{tot}, correspond to $\Delta I=0$ (unstretched) and $|\Delta I|=1$ transitions, respectively. The angular distribution of these components is, in the center of mass frame of reference (i.e after the Doppler shift correction), given by

$$W^{|\Delta I|=1}(\theta,E_\gamma)=W_0(E_\gamma)[1-\frac{1}{4}P_2(\cos\theta)] \tag{15}$$

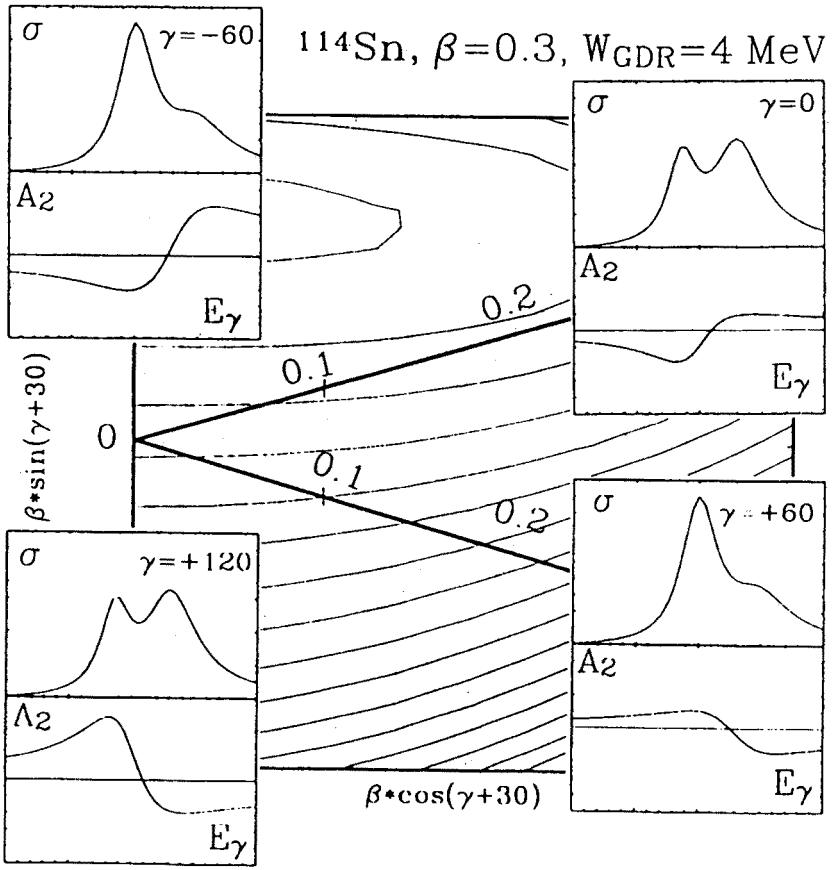

Figure 8: Schematic illustration of expected GDR strength function and angular distribution for various shapes of the same deformation. This calculation is for ^{114}Sn.

and

$$W^{\Delta I=0}(\theta,E_\gamma)=W_0(E_\gamma)[1+\frac{1}{2}P_2(\cos\theta)] \qquad (16)$$

Here P_2 is a Legendre polynomial in the polar angle θ between the direction of emission of the gamma ray and the beam axis. In experiments where the direction of the angular momentum can be determined, for example from a measurement of the plane of a subsequent fission reaction, the angular distribution of the gamma rays with respect to the direction of the angular momentum vector (normal to the fission plane) is given by

$$W^{|\Delta I|=1}(\vartheta,E_\gamma)=W_0(E_\gamma)[1+\frac{1}{2}P_2(\cos\vartheta)] \quad (17)$$

and

$$W^{\Delta I=0}(\vartheta,E_\gamma)=W_0(E_\gamma)[1-P_2(\cos\vartheta)] \quad (18)$$

The larger amplitudes for the latter case reflect the increased sensitivity arising from the fact that it is not necessary to average over the azimuthal orientation of the angular momentum vector.

In an oblate nucleus, rotating non-collectively, the two longer axes give rise to two degenerate components at lower transition energy, both with $|\Delta I|=1$, while the shorter symmetry axis, being parallel to the direction of I_{tot} now corresponds to a vibrational component with $\Delta I=0$. In experimental analyses, the data are normally fitted to the function $W(\theta,E_\gamma)= W_0(E_\gamma).(1+A_2(E_\gamma)P_2\cos(\theta))$. The resulting pattern of the $A_2(E_\gamma)$ coefficients in the GDR energy region is therefore sensitive to the magnitude of the deformation, since the components with different angular distributions will have different overlaps according to the size of the deformation, and to the shape and orientation of the density distribution. The latter effect is illustrated in figure 8, which shows calculated angular distribution patterns for 4 different shapes of the nucleus ^{114}Sn for a given deformation. It is seen that nuclei with prolate shapes rotating collectively and oblate nuclei rotating non-collectively have similar angular distribution patterns, although the amplitude is lower for the prolate case. For prolate nuclei rotating non-collectively and oblate nuclei rotating collectively, the sign of the $A_2(E_\gamma)$ pattern is reversed, as is the amplitude relation, due to the inversion of the axes with respect to I_{tot}.

All measurements of the angular distribution pattern in the GDR region, made to date, are consistent with nuclear shapes in the sector of prolate shapes rotating collectively and oblate shapes with the angular momentum aligned along the symmetry axis. In situations where shape fluctuations are important, the amplitude of the A_2 can be significantly attenuated due to the changing overlap of the various vibrational components. Likewise, if I_{tot} is not perpendicular to one of the major axes, the angular distribution will be attenuated.

2.3.2 An overlooked effect.

We will discuss results from GDR angular distribution measurements in more detail in section 3. Here we take the opportunity to point out that in all the analyses carried out so far of experimental angular distributions the effect of the phase space on the fine structure of the GDR transitions has been neglected when comparing theory to experiment.

The basic idea is very simple. A GDR consists of 5 major components corresponding to gamma ray transitions with $\Delta I=-1,0,+1$ (see table 1). Since the decay probability from a given state depends on the density of the states that the decay may proceed to (see equations 1 and 7) it is clear that the decay of the GDR components will not be equally probable if the density of final states are different. Equation 2 tells us that this is indeed the case due to the angular momentum dependent rotational energy.

Although we are dealing with small differences in I, the effect will be particularly large in relative terms if the initial state lies at low excitation energy above the yrast line and if the nucleus has a small moment of inertia (large rotational energy). Figure 9 illustrates the situation. We have in this figure plotted typical yrast line energies nuclei with masses 45, 60,

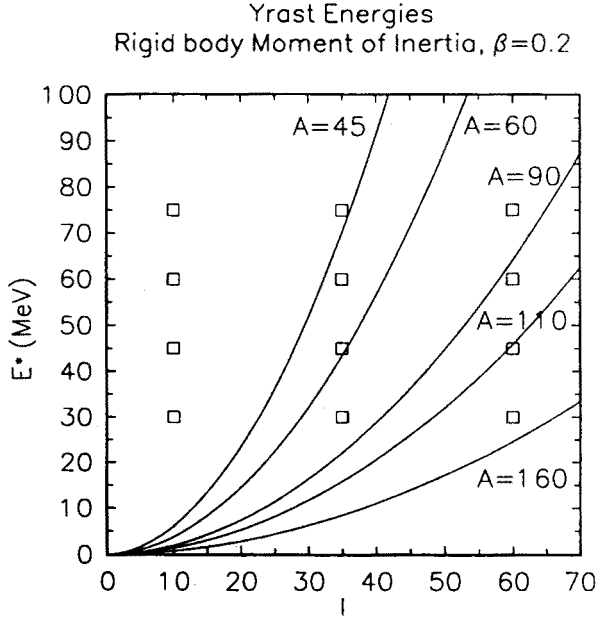

Figure 9: Illustration of the available thermal energy available for GDR excitation in nuclei of different masses.

100 and 160. It is seen that in reactions forming lighter nuclei with excitation energies in the range E^*=40-80 MeV one may be very close to the yrast line even at moderate angular momenta.

In figure 10 we show the effect of including the varying density of levels for the ΔI=-1,0,+1 GDR transitions, according to equation 2. The calculation proceeds as a miniature statistical model by assigning to each of the (in general 5) GDR components a Lorentzian shape centered at the energies given in table 1 and a width that scales with the centroid energy as a power law ($\Gamma=\Gamma_0(E/E_0)^\delta$; δ=1.9). The unperturbed transition strengths of these components were also taken from table 1. At each transition energy the actual decay strength is then taken as the product of the unperturbed strength and the density of the final levels at that excitation energy and spin. Since each of the GDR components is labelled by its ΔI, the angular distribution effect can be taken into account. We have in this simple model neglected the competion with neutrons (particles), since we are not interested in reproducing the absolute decay probability (this argument assumes that $\Gamma_\gamma/\Gamma_{tot} = \Gamma_\gamma/(\Gamma_n + \Gamma_\gamma) \approx \Gamma_\gamma/\Gamma_n$, which is indeed the case for gamma ray at GDR transition energies).

From the discussion in the previous section it is obvious that the magnitude of the effect depends on the nuclear shape (as given by the parameter γ). For example the effect is particularly important for prolate nuclei for which the upper part of the GDR consists of a mixture of ΔI=0 and ΔI=±1 transitions. A suppression of the ΔI=+1 transition strength then affects the measured angular distribution in the part of the spectrum where mixed multipolarities are present. This is indeed what is seen in figure 10, where we exhibit calculated angular distributions for nuclei of various masses but of the same deformation β for various initial conditions (E(excitation)=E(thermal)+E(rotation) and I). As expected we see that when the thermal excitation energy is high the distortion of the $A_2(E_\gamma)$, as compared to the limit where level density effects are neglected, is small. This is normally the situation for the heavy-ion

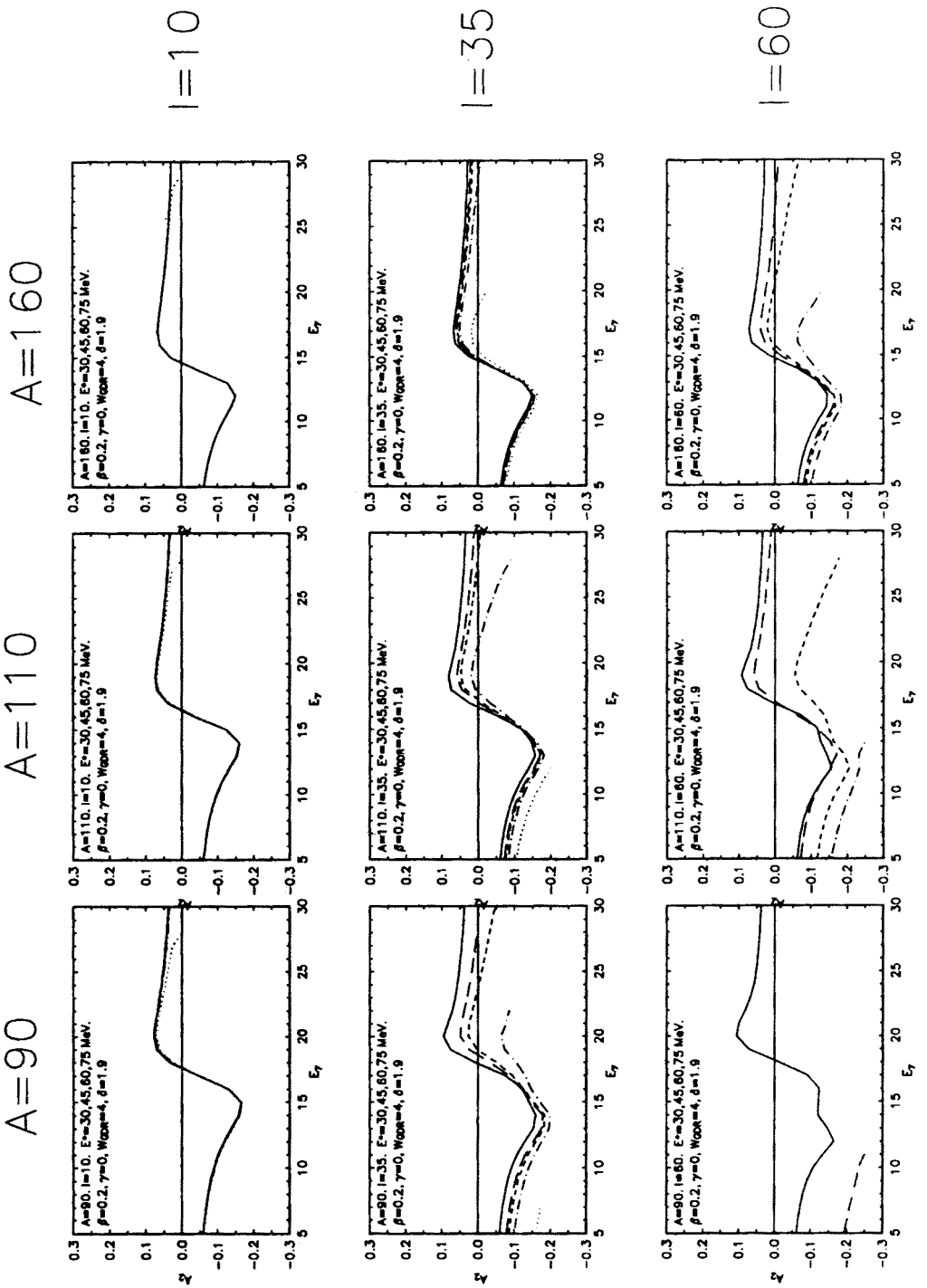

Figure 10: Calculated distortion of GDR angular distributions due to density of final states. The initial excitation is: 75 MeV (long dashed), 60 MeV (short dashed), 45 MeV (dot dashed), 30 MeV (dotted), effect neglected (solid line)

induced reactions that lead to the formation of heavy nuclei (A>100) except perhaps at the highest spins. In light nuclei however many studied reactions lead to the formation of compound systems with moderate excitation energies but rather high angular momenta. An example of anomalous GDR angular distributions in hot and rotating ^{45}Sc nuclei have been presented by Marta Kicinska-Habior at this school[15,16]. The observed behaviour is in qualitative agreement with the results of the present model investigation. In figure 11 we show how the GDR strength function is affected by the level density effect. It is seen that also the strength function can be significantly affected by level density effects in lighter nuclei. We mention that the usual statistical model analysis of GDR spectra with CASCADE does not treat this effect. CASCADE treats the GDR as a single entity, not as components corresponding to different ΔI values. Thus fits to experimental GDR spectra neglecting these effects may

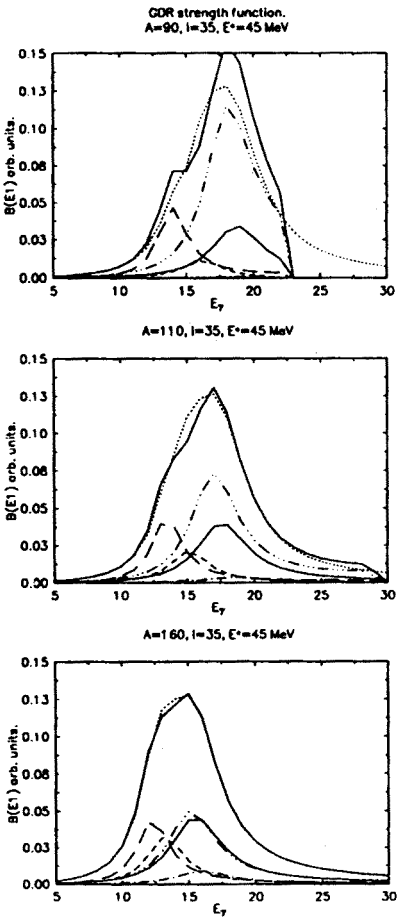

Figure 11: Calculated GDR strength functions including the influence of the different level densities for ΔI=-1,0,+1 transitions. Solid line: level density effect included. Dotted line: effect neglected.

lead to significant errors in the analysis.

Finally, we mention that since the distortion of angular distributions depends on the nuclear shape, detailed comparisons between light-nuclei data and calculations including the effects pointed out here may provide additional sensitivity to the shape and deformation of the gamma ray emitting nucleus.

2.4 The shapes of hot nuclei.

We have mentioned that hot nuclei normally do not have a well defined shape as it is the case at low excitation energies. This is apparent from figures 12 and 13 which show the contours of the free energy of a hot and rotating nucleus in a polar representation in the variables β and γ. Theoretical studies of shape probability distributions at high excitation energy have normally been done in the canonical ensemble characterized by the variables temperature (T) and rotational frequency (ω) in terms of the free energy in the rotating frame

$$F = E - TS - \vec{I}\vec{\omega} \tag{19}$$

where S is the entropy. F can be calculated microscopically using standard mean field methods.

Of particular practical usefulness has been the development of a formalism based on the Landau theory of phase transitions[17] which in a simple form reveals the global features of the shape landscapes. In this approach, the free energy at a given T and ω is parametrized in terms of the deformation parameters, using coefficients which vary smoothly with temperature,

$$\begin{aligned} F(T,\omega,\beta,\gamma) &= F(T,\omega=0,\beta,\gamma) - \frac{1}{2}J_z\omega^2 \\ &= F_0(T) + A(T)\beta^2 - B(T)\beta^3\cos(3\gamma) + C(T)\beta^4 - \frac{1}{2}J_z\omega^2 \end{aligned} \tag{20}$$

where ω is the rotational frequency (here assumed to coincide with the z axis) and J_z the moment of inertia about the axis of rotation

$$J_z = J_0(T) - 2R(T)\beta\cos\gamma + 2J_1(T)\beta^2 + 2D(T)\beta^2\sin^2\gamma \tag{21}$$

For actual cases the temperature dependent coefficients F_0, A, B, C, J_0, R, J_1 and D must be determined by a fit to a full microscopic calculation.

The equilibrium shape at a given (T,ω) is then the one that minimizes F. The transition to the variables (E^*,I) can be effectuated using the expressions $T \approx (E^*/A)^{1/2}$, where a is the level density parameter, and from $I = J_{rig}\omega$, assuming either the rigid body moment of inertia or using an effective moment of inertia for the shape ensemble.

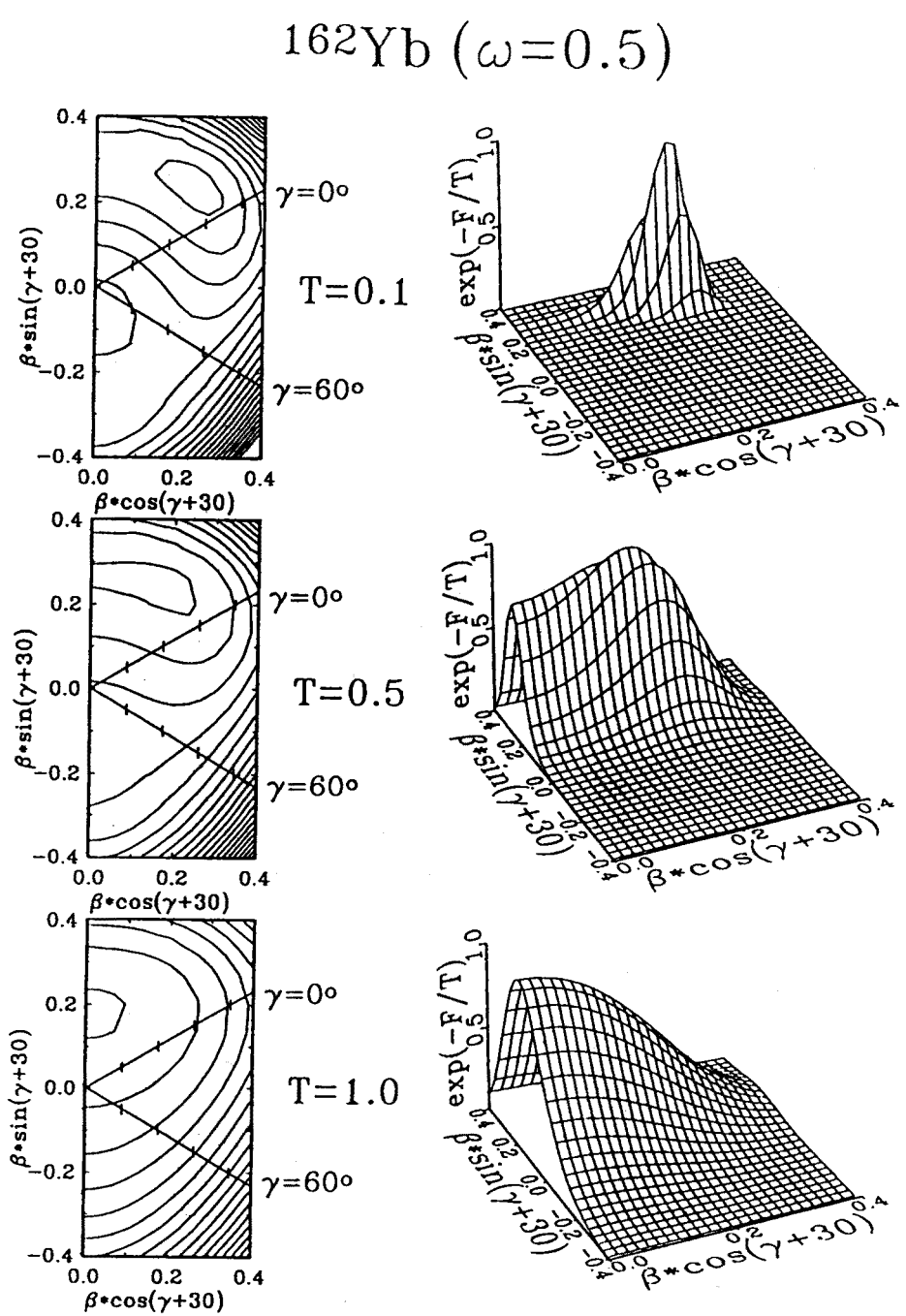

Figure 12: Contours of the free energy in the rotating frame calculated for the nucleus ^{162}Yb at ω=0.5 MeV and at T=0.1,0.5,1.0 MeV. The associated shape probabilities are shown on the right.

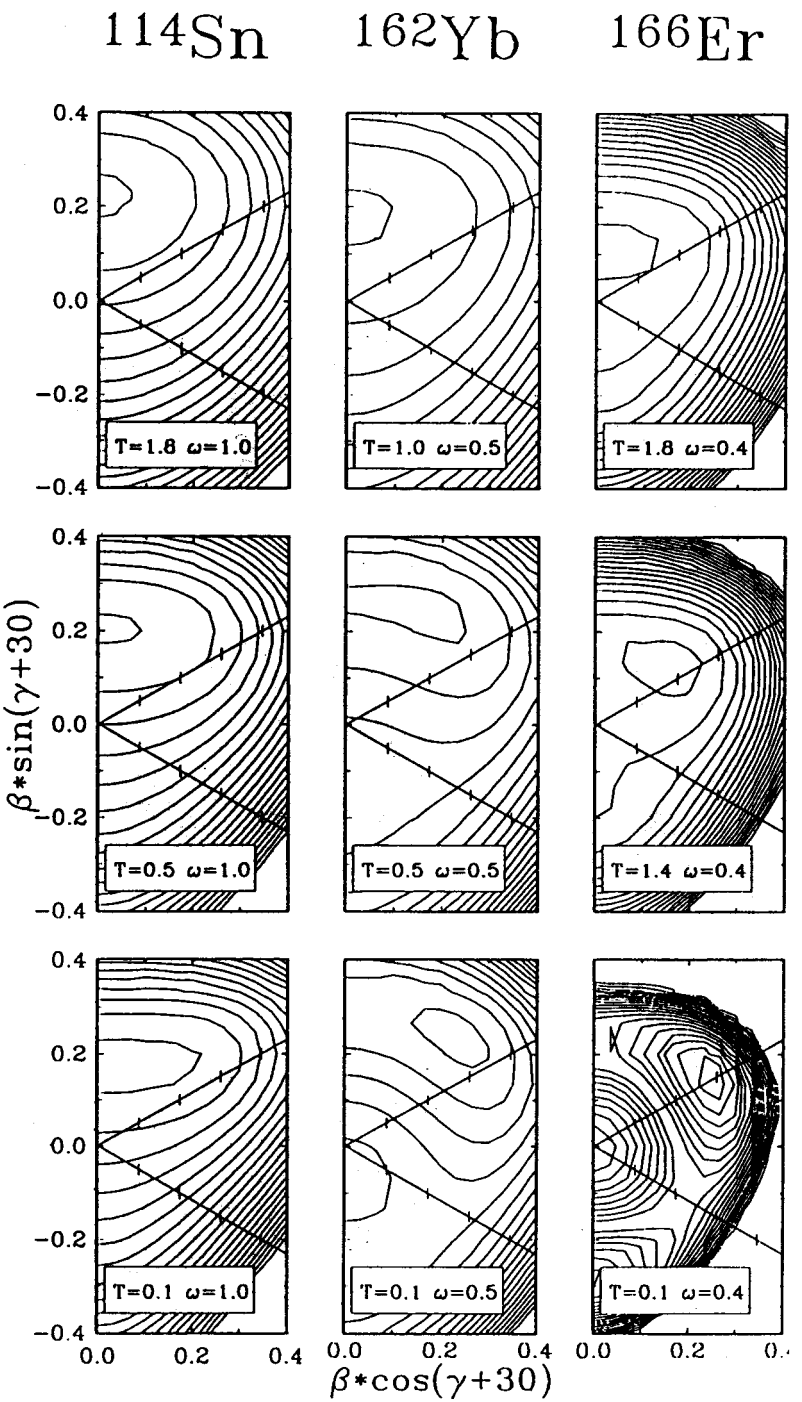

Figure 13: Contours of the free energy in the rotating frame for Sn, Yb and Er isotopes for various temperatures and for rotational frequencies corresponding to the same angular momentum (approximately I= 35).

2.5 Adiabatic shape fluctuations.

We are now armed to describe the expected effective GDR distributions in the case of fluctuations. The approach follows from standard statistical mechanics. For a system at constant temperature the probability that the nucleus has a deformation and shape (β,γ), in terms of the probability of having the equilibrium shape (β_0,γ_0) is given by

$$\frac{P(T,\omega,\beta,\gamma)}{P(T,\omega,\beta_0,\gamma_0)} = \exp[\frac{-[F(T,\omega,\beta,\gamma)-F(T,\omega,\beta_0,\gamma_0)]}{T}] = \exp(\frac{-\Delta F}{T}) \tag{22}$$

Such shape probability distributions for the nucleus ^{162}Yb are displayed in the right hand side of figure 12. They demonstrate that even at moderate temperature shape fluctuations are very important, and that they to a large extent obscure the shape phase transition predicted for the equilibrium deformation.

For the GDR, the simplest approach consists in assuming that during the time it takes for a GDR to build up and to subsequently decay the nuclear shape does not change. This is the *adiabatic approximation.*

In this picture, the effective GDR strength distribution, measured in experiment, is a sum of the strength distributions corresponding to vibrations built on each of the shapes that the nucleus can explore, weighted with the probability that the nucleus has that shape,

$$<f_{GDR}(E_\gamma,T,\omega)> = \frac{\int f_{GDR}(E_\gamma,\omega,\beta,\gamma)e^{-F(T,\omega,\beta,\gamma,\theta,\phi,\psi)/T}d\tau}{\int e^{-F(T,\omega,\beta,\gamma,\theta,\phi,\psi)/T}d\tau} \tag{23}$$

Here f_{GDR} denotes the GDR strength function, defined by equation 7 with the exception of the exponential factor, and calculated in the harmonic oscillator model or in some more elaborate model.

The volume element $d\tau$ is associated with the quadrupole parameters β, γ, θ, ϕ and ψ. The last 3 variables are the Euler angles describing the orientation of the nucleus with respect to the direction of the angular frequency vector. The volume element follows from the Jacobian expressing the transformation from the general 5 quadrupole variables to the particular set used above metric

$$d\tau = \beta^4 |\sin(3\gamma)| \sin(\theta) d\beta d\gamma d\theta d\phi d\psi \tag{24}$$

The averaging should be done over an interval $\Delta\gamma$=60 degrees, covering shapes ranging from prolate to oblate, in order not to include an implicit averaging over the orientation degrees of freedom (see below).

Equation 20 is modified to

$$F(T,\omega,\beta,\gamma,\theta,\phi)=F(T,\omega=0,\beta,\gamma)-\frac{1}{2}(J_x\sin^2\theta\cos^2\phi+J_y\sin^2\theta\sin^2\phi+J_z\cos^2\theta)\omega^2 \qquad (25)$$

where J_x, J_y and J_z denote the intrinsic moments of inertia for the principal axes. This formulation once again assumes that the GDR couples adiabatically to the orientation degrees of freedom.

Neglecting the effect of the Coriolis splitting on the GDR components an analytical expression for the angular distribution, with respect to the beam axis, can be derived[18]

$$a_2(E_\gamma)=-\frac{1}{2}\frac{(f_x(E_\gamma)+f_y(E_\gamma))/2-f_z}{f_x+f_y+f_z}\frac{3\cos^2\theta-1}{2}+\frac{3}{8}\frac{f_x-f_y}{f_x+f_y+f_z}\sin^2\theta\cos(2\phi) \qquad (26)$$

where f_x, f_y, f_z are the absorption cross section distributions for the GDR along the principal axes of the nucleus.

A few words of caution concerning this approach is appropriate. Indeed, the discussion above has been carried out in terms of the canonical variables T, and ω, and not in the physical variables E^* and I. The differences arising in the treatment of shape fluctuations from conserving T constant and not E^* have been explored by Goodman[19]. Since the available energy is constantly repartitioned between the thermal energy and the deformation energy, deformations away from equilibrium are less populated since the thermal energy is reduced. In particular, at low E^*, the temperature vanishes for large deformations as may be seen from the Fermi gas expression for the temperature

$$T=\sqrt{\frac{E^*-b(\beta-\beta_0)^2}{a}} \qquad (27)$$

In the expression above, a quadratic dependence of the deformation energy on the quadrupole shape parameter β has been assumed. In contrast, all shapes are populated with the constant temperature constraint. The constant energy constraint can be treated by expressing the shape probability not in terms of the free energy as in equation (22), but in terms of the entropy

$$\frac{P(E,I,\beta,\gamma)}{P(E,I,\beta_0,\gamma_0)}=\exp[S(E,I,\beta,\gamma)-S(E,I,\beta_0,\gamma_0)]=\exp(\Delta S) \qquad (28)$$

The equilibrium shape is the one that maximises the entropy. The differences have been explored quantitatively for the nucleus ^{166}Er. It is found that the shape probability distributions are not altered significantly for E*> 30 MeV, although the constant T constraint in general gives broader shape probability distributions.

The differences between the constant rotational frequency constraint and the more physical constant angular momentum constraint has also recently been explored by Goodman for the Landau model and in microscopic calculations, based on a two dimensional cranking model

for a single j shell (j=13/2). For each orientation the rotational frequency is varied in order to maintain the same average I. An issue here is whether, at finite T, the moments of inertia about the principal axes are affected by orientation fluctuations. For a classical rotating rigid body the moments of inertia will not be affected, but for a rotating nucleus this is not necessarily the case. In the Landau model, using the following relation between I and ω

$$\begin{aligned} I(I+1) &= I_x^2 + I_y^2 + I_z^2 \\ &= (J_x\omega_x)^2 + (J_y\omega_y)^2 + (J_z\omega_z)^2 \end{aligned} \tag{29}$$

the orientation probability distribution is

$$\begin{aligned} P(T,I,\beta,\gamma,\theta,\phi) &\propto \exp[-\frac{E-TS}{T}] \\ &= \exp[-\frac{1}{T}(F(T,\omega=0,\beta,\gamma) + \frac{1}{2}\sum_{i=x,y,z} J_i\omega_i^2)] \\ &= \exp[-\frac{1}{T}(F(T,\omega=0,\beta,\gamma) + \frac{J_x\sin^2\theta\cos^2\phi + J_y\sin^2\theta\sin^2\phi + J_z\cos^2\theta}{J_x^2\sin^2\theta\cos^2\phi + J_y^2\sin^2\theta\sin^2\phi + J_z^2\cos^2\theta}\ \frac{I(I+1)}{2})] \end{aligned} \tag{30}$$

It is found that the constant ω constraint may significantly overestimate the orientation fluctuations at finite temperature as compared to the constant I constraint. However, these issues have not yet been explored in detail as far as the observable effects on the GDR angular distribution are concerned.

2.5 Dynamical fluctuations.

In the previous section we have discussed the adiabatic situation, disregarding that the coupling of the GDR to the shape degrees of freedom may depend on the relative time scales of the collective shape and vibrational motions therefore requiring a dynamical treatment. The idea[20] is the following. With increasing temperature the time spent by the excited nucleus in a configuration characterized by a given deformation and orientation, decreases. Hence, the nucleus may not spend enough time in a given point in deformation space for the GDR to adjust its frequency to the shape. Rather, the jumping between different shapes implies that the GDR never explores the extreme deformations but feels only the average shape. Such a mechanism would substantially reduce the effect of shape and orientation fluctuations.

The proposed effect, called *motional narrowing*, is a nuclear analog to that responsible for the narrowing of the line shape in the nuclear magnetic resonance (NMR). It occurs whenever a periodic resonant effect undergoes a random time-dependent perturbation occurring on a time scale shorter than the time needed for the system to adjust its frequency to that perturbation. In the NMR case, the relevant time scales are those relevant for a change of the magnetic field at a given lattice point in a crystal, due to the temperature dependent mobility of neighbouring atoms, relative to the time needed to adjust to a change of the field. In nuclei the relevant parameters are the inverse of the hopping time between different shapes ($\Gamma = \hbar/\tau$) and the quantity $\delta\omega$ measuring the spread in dipole frequencies corresponding to different nuclear shapes. If $\delta\omega \ll \Gamma$, motional narrowing will occur. If we take $\delta\omega$= 1-2 MeV for fluctuating nuclei, we obtain typically $\tau \approx 5\times10^{-22}$ sec. Hence, an experimental determination of the validity of the motional narrowing picture could provide new information on the characteristic

time scales for shape rearrangements in hot nuclei.

These issues, and the consequences for the GDR have recently been explored quantitatively by several authors. Alhassid and Bush[21] have described the time evolution of the quadrupole shape parameters α in terms of a Langevin equation

$$\frac{\partial \alpha}{\partial t} = -\frac{1}{\chi}\frac{\partial F}{\partial \alpha} + f(t) \tag{31}$$

where f is a random force which causes statistical fluctuations in the shape parameters and make the process stochastic. χ is a parameter which scales the driving force for α and which is a measure of the degree of adiabaticity, being proportional to the average relaxation time of the quadrupole motion.

Ormand et al.[22] have described the jumping in terms of a Kubo-Anderson process. In this model the conditional probability of having a given deformation α at time t after having been at α_0 at time t_0 is written

$$P(\alpha,t|\alpha_0,t_0) = e^{-\Gamma(t-t_0)}\delta(\alpha-\alpha_0) + (1-e^{-\Gamma(t-t_0)})e^{-F/T}\left(\int e^{-F/T}d\tau\right)^{-1} \tag{32}$$

where Γ is the mean shape jumping rate. In both cases the quadrupole coordinates α include both shape and orientation degrees of freedom. In an extended formulation the shape and orientation coordinates have been treated separately allowing for the possibility that the relaxation time for the shape and orientation degrees of freedom may be different.

The influence on the GDR spectrum and angular distribution from these various types of fluctuations are displayed in figure 14.

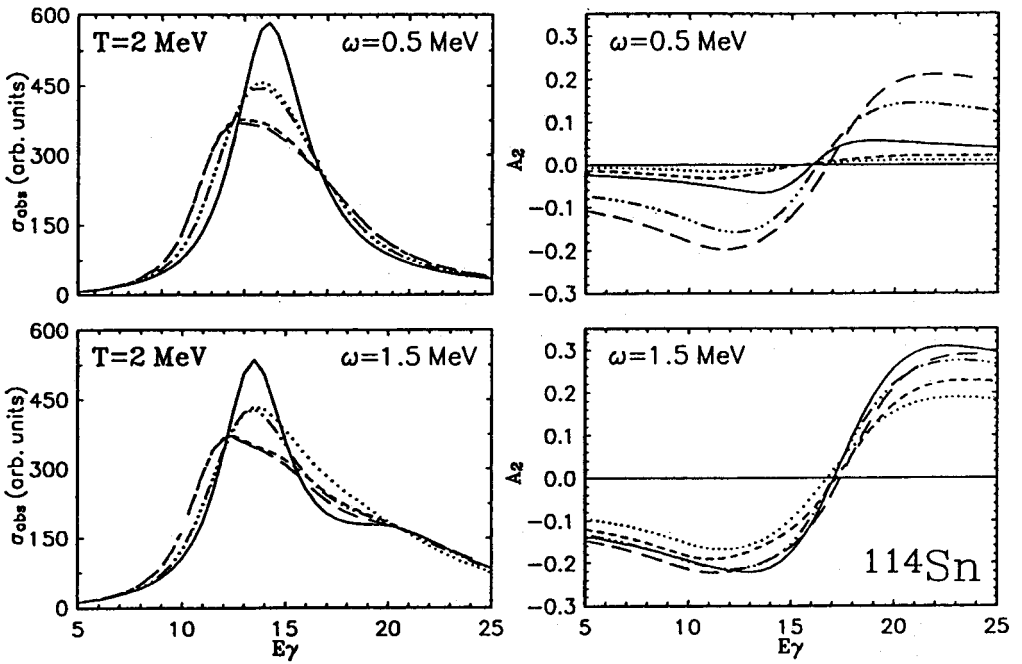

Figure 14: Effect of shape and orientation fluctuations on the strength function and angular distribution of the GDR. Solid: no fluctuations. Long-dashed: adiabatic shape fluctuations. Short dashed: adiabatic shape and orientation fluctuations.

3. UNDERSTANDING THE GDR WIDTH FROM E*= 40 MeV to 600 MeV.

We now return to a discussion of figure 6. As mentioned earlier this figure is the paradigm for GDR's in excited nuclei. Understanding these systematics provides quite a lot of insight into the properties at finite temperature of a finite numbered many body system consisting of identical particles, which is what a hot nucleus is. The concepts presented in section 2, provide the basis for such an understanding. Of course, this discussion has proceeded in conflict with chronology. In real life all the nice formulas and pedagogical presentations normally come much after the discovery of the basic facts, which of course is why its fun to do experiments. In the following talk Pier Francesco Bortignon will also discuss the systematics of the GDR width in some detail, but from a more deep-rooted theoretical point of view.

3.1. The increase of the GDR width up to $E^* \approx$ 130 MeV.

A striking feature seen in figure 6 is the strong increase of the GDR width seen in the Sn isotopes when the excitation energy of the compound nucleus increases. Indeed the width increases from the ground state width ($\Gamma_{GDR}(T=0) \approx$ 5 MeV) to about 12-13 MeV at E^* =120 MeV. Above that value the experimentally determined width does not appear to increase any more (we will return to this in the following subsection). We mention that all the experiments underlying the data points in this figure were coincidence experiments in which the gamma ray spectra were measured in coincidence with either the recoiling fusion products or with the detection of a minimum number of low energy gamma rays originating from the residues. As such the fusion character of the reactions was well determined and thus also the initial conditions for the statistical model analysis.

There is one important point which must be remembered when looking at figure 6. That is that in heavy ion fusion reactions any increase in the kinetic energy of the beam and therefore also of the excitation energy of the compound nucleus is also accompanied by an increase in the angular momentum. This is shown in the lowest panel in figure 6. It is apparent that the angular momentum of the compound nucleus increases strongly as the excitation energy also increases. One might therefore suspect that angular momentum effects could well play an important role in the observed width increase. A priori it is a difficult experimental task to separate the effects due to angular momentum from those due to excitation energy.

We may turn to calculations for a while. From the calculations of the free energy surfaces one may estimate the broadening of the GDR strength function due to thermal shape fluctuations assuming the fully adiabatic model described in section 2.5. In this model it turns out that the width broadening goes roughly as

$$\delta\Gamma = 1.3\sqrt{T} \tag{33}$$

This is obviously too weak a temperature dependence to reproduce the observations. We may then ask about the role of the angular momentum. Calculations of the free energy surfaces of excited and rotating Sn nuclei give us the possibility of following the evolution of the equilibrium shape with increasing E^* and I. Such calculations indicate that the equlibrium shape rapidly becomes oblate even at T<1 MeV, with a deformation which increases with spin (see figure 15), as expected for centrifugal stretching of a rotating liquid drop. If the deformation increases, the GDR peaks move apart and the overall width of the

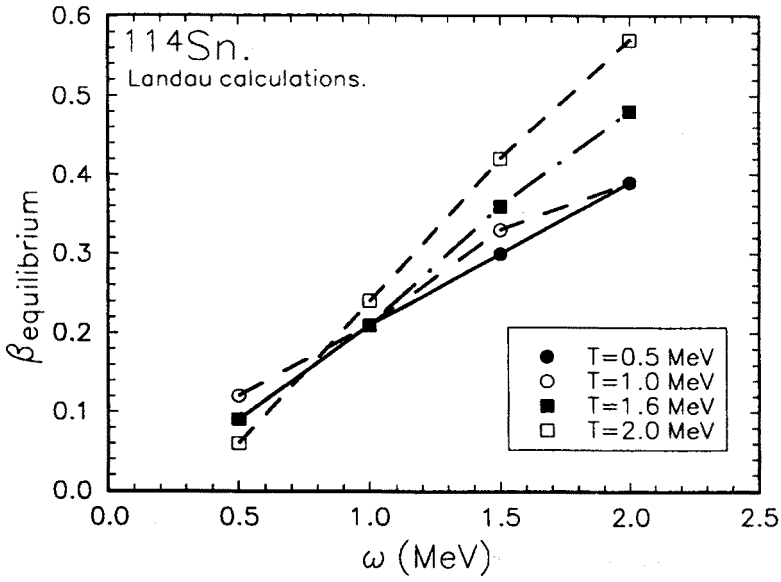

Figure 15: Evolution of the equilibrium deformation β as a function of the angular momentum for ^{114}Sn.

GDR increases. A number of such calculations have been carried out which can reproduce the trend of the observed increase of the GDR width in the Sn isotopes. Although it has been found that a fully adiabatic shape averaging tends to overpredict the GDR width. In contrast a rather good description is obtained assuming that the coupling of the GDR to the shape degrees of freedom is intermediate between the motional narrowed regime and the fully adiabatic regime. Thus present day calculations of the shapes of hot nuclei suggest that the observed GDR width increase is mainly due to angular momentum induced deformation changes.

The measurement of the angular distribution of the GDR gamma rays provides an additional testing ground for these ideas. In recent experiments with the HECTOR array (described in the contributions of Adam Maj and Franco Camera to this meeting, and also shown in figure 16) we have investigated the angular momentum and temperature dependence of the GDR angular distribution. The measured $A_2(E_\gamma)$ values[23] plotted as a function of the compound nucleus angular momentum are shown in figure 17. The main feature is the systematic increase of the $A_2(E_\gamma)$ observed with increasing angular momentum. Similar effects are also observed in other mass regions. An interesting observation is that very similar distributions are observed in a reaction producing Sn nuclei at 15 MeV lower excitation energy supporting the idea that the excitation energy is not the main driving force. Also show in the figure are $A_2(E_\gamma)$ distributions calculated assuming fully adiabatic shape and orientation averaging (full drawn lines) and full motional narrowing (dashed). The latter is taken as the equilibrium value. It is seen that while in general the calculations are able to reproduce the data rather well, a closer inspection exhibits some discrepancies. This is more apparent in figure 18 where we plot A_2 values in the interval $11<E_\gamma<14$, i.e. around the minimum of the $A_2(E_\gamma)$ distribution. It may be seen that the adiabatic calculation reproduces the data well at the lower spins, while the motional narrowed calculation agrees with the high spin points. It may also be noted that none of the calculations reproduce the trend of the data points. This might at first seem

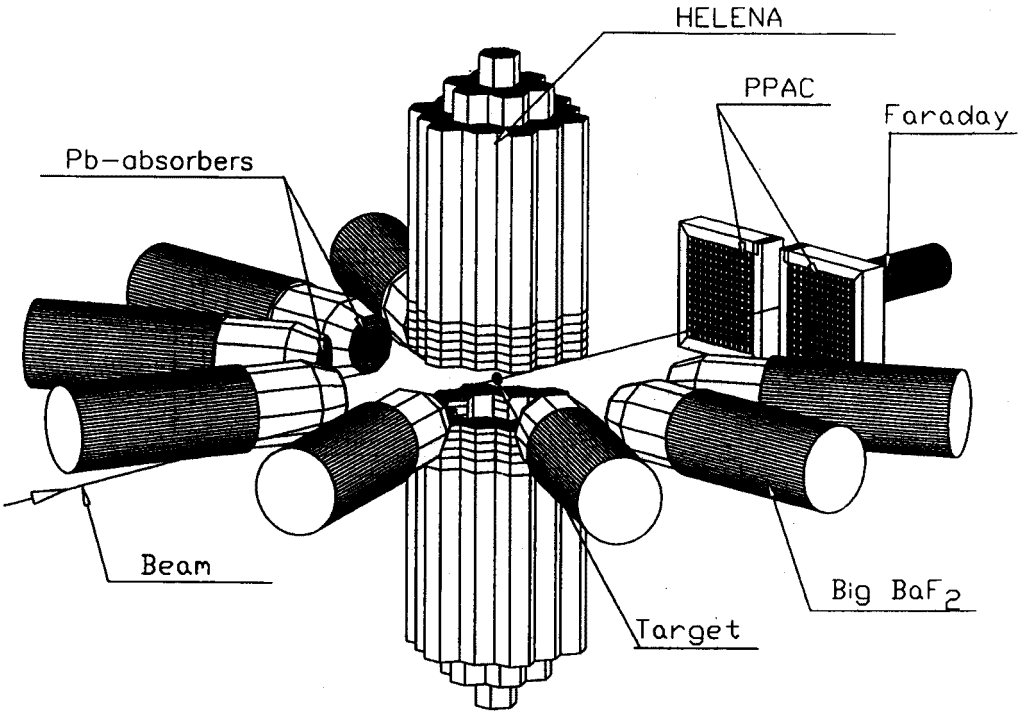

Figure 16: HECTOR, a Danish-Italian collaboration, consists of a multiplicity array of 38 BaF_2 (shown in a opened state) and 8 large BaF_2 scintillators for measuring high energy photons from excited nuclei.

surprising considering the predicted deformation increase. Part of the explanation may be that the dominant effect in the observed increase of $A_2(E_\gamma)$ is due to orientation fluctuations.

Nevertheless it appears clear that we do not have at the present time a theory which is able to explain all the details of the phenomena we observe in the new generation of exclusive experiments we have discussed here.

The most comprehensive data set is available for the Sn isotopes. We are at present also investigating nuclei in the heavy rare earth nuclei ($^{165\text{-}167}$Er, $^{161\text{-}160}$Yb, $^{174\text{-}175}$Hf isotopes) using spin and energy differential techniques. Some of these results are discussed in the contribution of Adam Maj to this school[24] and of Franco Camera. We remark that the interest in this mass region is that these nuclei have strong shell structure driven ground state deformations. The isotopes with neutron numbers around N=90 are softer, rapidly becoming oblate with increasing temperature, while the Hf isotopes (N=102-104) are expected to conserve the prolate ground state shapes up to T≈1.8 MeV (about 70 MeV in this mass range).

The experimental observation that the GDR width in the Sn isotopes saturates at excitation energies above $E^* \approx 130$ MeV is in fact consistent with angular momentum effects as the main reason behind the GDR width increase. Indeed the angular momentum cannot continue to grow as the excitation energy increases due to the onset of fission. The lower panel in figure 6 shows that the transferred angular momentum increases with increasing excitation energy (and thus also bombarding energy) and saturates at about $I \approx 60$. This occurs at about the same excitation energy as the observed saturation of the width.

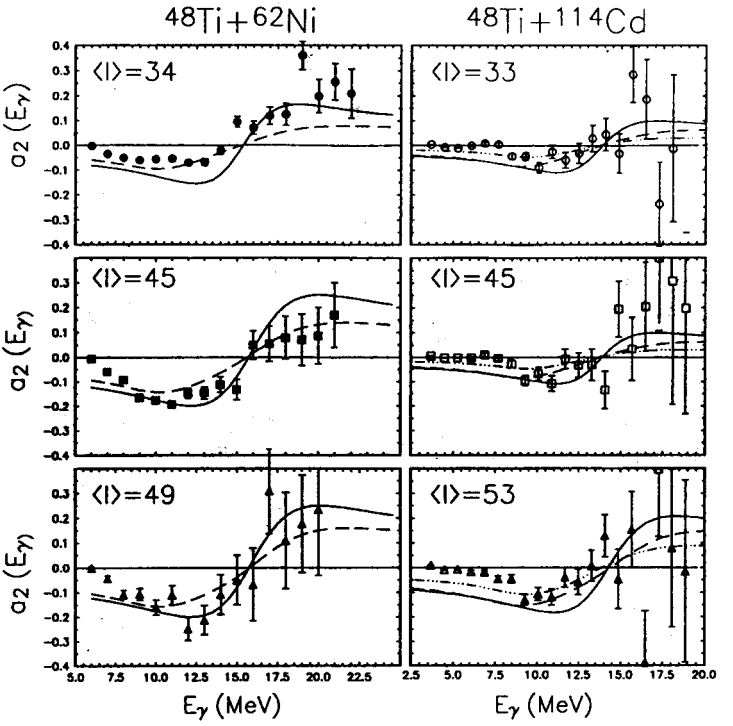

Figure 17: Measured angular distribution for Sn and Yb as a function of the angular momentum. Calculations: adiabatic model (dashed line), extreme motional narrowing (solid line) corresponding to the equilibrium deformation..

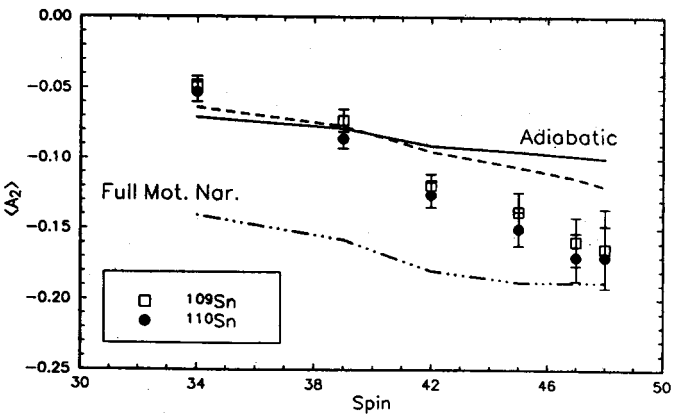

Figure 18: Plot of the A_2 in the interval 11-14 MeV as a function of the angular momentum of the emitting nucleus. Calculations show the predictions of the adiabatic and the extreme motional narrowing models.

3.2 The saturation of the GDR width at E>130 MeV and the vanishing of the gamma emission strength at E*>350 MeV.*

There are two characteristic features which develop as the excitation energy of the compound nucleus is raised, as may be seen in figure 6. One is the constancy of the GDR width, the other is the vanishing of the gamma ray strength in the GDR energy range. This appears to set in at E^*> 350 MeV. The two features may well be related as we discuss below.

In the analysis of the 10,15 and 19 MeV/u reactions leading to the formation of excited Sn isotopes, the gamma ray spectra were reasonably well reproduced by statistical model calculations for which the GDR width was about Γ_{GDR}=13 MeV. Even for the 24 MeV/u reaction, it appears that the width is less than 15 MeV. These values are consistent with a modest influence on the GDR arising from temperature effects, (see equation 33), as discussed above.

Support for this point of view is also provided by recent measurements of the high energy photon emission from deeply inelastic reactions of $^{136}Xe+^{48}Ti$ at 18 MeV/u[25]. Here, the GDR gamma ray spectra were correlated with the total kinetic energy loss, as determined by a measurement of the direction and velocity of the fragments. The analysis of the spectra with the statistical model, indicates that emission from the Xe like fragments dominates and that the width of the GDR saturates to $\Gamma_{GDR}\approx$ 10 MeV above $E^*/u\approx$ 1 MeV (i.e. around $E^*\approx$ 130 MeV). This observation thus agrees well with the results obtained in the Sn region.

There are theoretical estimates of the temperature dependence of the spreading width, $\Gamma^{\downarrow}$, of the GDR that support this interpretation. The coupling between the GDR and the low lying 2p-2h states has been studied and found to be roughly independent of temperature. In his contribution P. F. Bortignon discusses some recent investigations which suggest that the constancy of the GDR width arises due to a cancellation of two effects: on one hand the coupling to the surface vibrations decreases with increasing T, while the collision widt increases somewhat with T.

In contrast to this point of view, the vanishing of the observable GDR strength at elevated temperatures can be phenomenologically explained by assuming that the GDR width grows rapidly with temperature, thereby spreading strength outside the region of transition energies E_γ=10-20 MeV. A problem is that strength outside the main GDR region is difficult to identify experimentally. At the low energy side of the GDR, the neutron threshold (around 10 MeV) limits gamma emission dramatically. At the high energy side, the bremsstrahlung contribution undermines a precise analysis. In a parametrization of the width in terms of the thermal energy , $\Gamma_{GDR}(E_x)= \Gamma_0 +0.036E_x+ 1.6\ 10^{-8}\ E_x^4$ was suggested and used in the statistical model analysis of experimental spectra from $^{40}Ar + ^{92}Mo$ reactions[26] at 21 and 26 MeV/A. With this procedure, the observed gamma ray multiplicities can be reproduced at all energies, as well as the GDR widths measured in A= 130 nuclei up to E^*= 120 MeV. However, this parametrization implies a very strong growth of the intrinsic GDR width at higher excitation energies. For example, $\Gamma(E^*=130)\approx$ 14 MeV and $\Gamma(E^*=250)\approx$ 75 MeV, implying strongly overdamped vibrations already at $E^*\approx$ 150 MeV. That aspect appears difficult to reconcile with the rather narrow GDR structures observed in experiments around that temperature (see figure 3 and 6).

Since the width for direct neutron emission is expected to be small ($\Gamma^{\uparrow}$< 1 MeV) such an increase would have to come about from a strong increase of the spreading width. A recent calculation based on the Vlasov equation with a relaxation time approximation using semiclassical methods predicts such a strong increase of the damping width with increasing T, due to nucleon-nucleon collisions[27]. By including the competition with particle emission

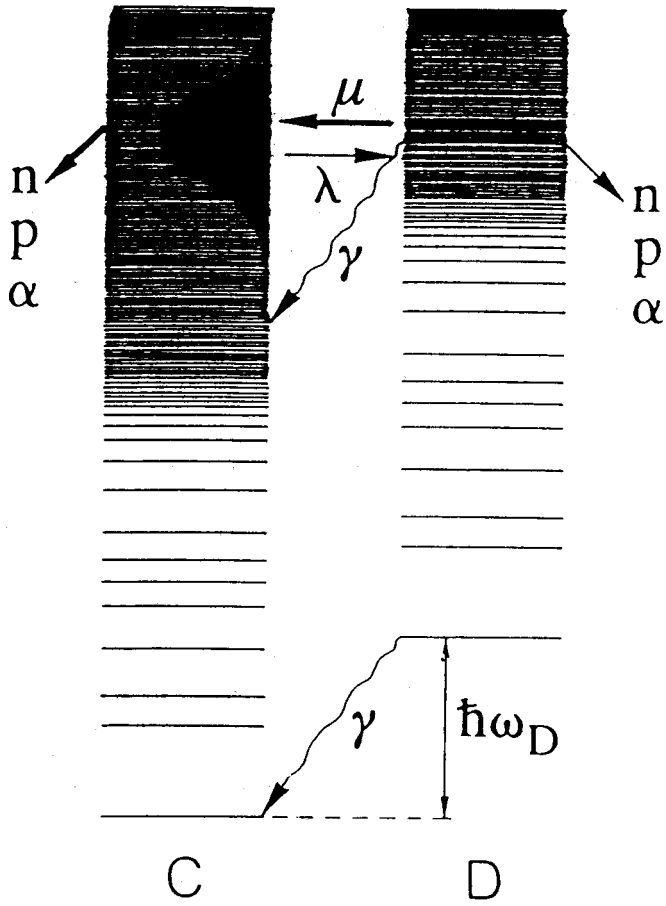

Figure 19: Illustration of schematic model used to discuss the GDR at high excitation energies as described in the text.

which depletes the initial excitation energy, a saturating behaviour of the apparent width is claimed. The strong increase in the role played by collisional damping predicted by this model seems however difficult to reconcile with the results of calculations of phase space models (based for example on Boltzman-Uhling-Uhlenbeck approaches). These have had notable success in explaining observed bremsstrahlung spectra.

Recently, general arguments have been advanced for a constancy of the GDR width as a function of temperature[28]. The idea is based on the expectation that, although equilibrium of the single particle degrees of freedom is attained rapidly ($\tau \approx 10^{-23}$ seconds) after only few collisions among the nucleons, the collective modes, like the GDR, only develop after some time. This time delay can be thought of as an equilibration time for the GDR, determined by the width of the coupling of the GDR to the other compound nucleus states. The temperature at which this width becomes comparable to the particle emission width defines a limiting temperature for the GDR decay. This problem has been investigated, as illustrated in figure 19, in a model comprising two classes of states, the compound nucleus states C, and the GDR states D. To each C state corresponds a state D shifted up by the energy of the GDR. The transition rates between these classes are denoted λ and μ.

From the principle of detailed balance the ratio λ/μ is equal to the ratio of the associated level densities

$$\begin{aligned}\frac{\lambda}{\mu} &= \frac{\rho_D}{\rho_C} \\ &= \frac{\rho_C(E^*-E_{GDR})}{\rho_C(E^*)} \\ &< 1\end{aligned} \tag{34}$$

Both classes of states can decay by particle emission, while only the dipole states can decay by high energy gamma emission. The time dependent probabilities for being in either class of states satisfy the equations,

$$\begin{aligned}\frac{dP_D}{dt} &= -(\mu+\gamma_\gamma+\gamma_{ev})P_D+\lambda P_C \\ \frac{dP_C}{dt} &= -(\lambda+\gamma_{ev})P_C+\mu P_D\end{aligned} \tag{35}$$

where γ_γ and γ_{ev} are the decay rates for gamma rays and particles, and $\lambda << \mu$ because of the different level densities. Assuming that the system starts in a state C the equations can be solved yielding

$$\begin{aligned}P_\gamma &= \frac{\gamma_\gamma}{\gamma_{ev}}\left(\frac{\lambda}{\gamma_{ev}+\lambda+\mu}\right) \\ &\approx \frac{\gamma_\gamma}{\gamma_{ev}}\left(\frac{\lambda}{\gamma_{ev}+\mu}\right)\end{aligned} \tag{36}$$

Below the critical excitation energy E_{crit}, $\gamma_{ev} << \mu$

$$P_\gamma(E^*<E_{crit}) = \frac{\gamma_\gamma}{\gamma_{ev}}\frac{\lambda}{\mu} \tag{37}$$

and well above this excitation energy, $\gamma_{ev} >> \mu$

$$P_\gamma(E^*>E_{crit}) = \frac{\gamma_\gamma\lambda}{\gamma_{ev}^2} < P(E^*<E_{crit}) \tag{38}$$

By equating the transition rate from the dipole states to the compound states to the GDR spreading width ($\approx$ 5MeV), and evaluating the temperature dependence of the particle widths a limiting excitation energy of the order of $E^* \approx$ 250 MeV can be calculated in good agreement with experiment. This interpretation establishes on a natural basis a time scale for the buildup of collective motion in hot quantum systems.

A final interesting idea due to V. Zelevinsky and P. F. Bortignon has been discussed by the

latter at this school. We refer to his talk for details, but just mention here that the main idea is that a constant GDR width (as a function of temperature) might indeed be expected for a system that has become fully chaotic (in the sense that all excitations are equally probable). Thus the constancy of the GDR width might sign the ultimate death of any dominating microscopic feature of the excited compound nucleus.

4. SUMMARY AND OUTLOOK.

We have in this talk attempted to give an impression of the many ways gamma rays from the decay of Giant Dipole Resonances can be used to investigate the properties of atomic nuclei excited to temperatures of billions of Kelvin. A central theme in present day research is the exploration of the time scales of such a hot system: the time of equilibration, the time for buildup of collective motion, the time for nucleonic rearrangements, the time for large scale mass rearrangements.

We have tried here to emphasize the importance of measurements of the angular distribution of the GDR photons as a useful tool. Although a reasonable understanding of many gross properties og excited state GDR's and of hot nuclei has now been obtained, it is also clear that much higher specificity and probably many unexpected features are waiting for us if we can cut up the (I, E^*) plane in small pieces and study them rather than integrating over large areas of this space. We have in the HECTOR collaboration undertaken such a program based on a new an powerful instrument and we look forward to much new exciting physics from it.

5. REFERENCES.

1. Permanent address: Nievodniczanski Institute of Nuclear Physics, Krakow, Poland.

2. Permanent address: Plysics department, University of Oslo, Blindern.

3. J. J. Gaardhøje. Annu. Rev. Nucl. Part. Sci. **42** (1992) 483-536.

4. K. A. Snover, Annu. Rev. Nucl. Part. Sci. **36** (1986) 545-603.

5. A. Bracco et al., Phys. Rev. Lett. **62** (1989) 2080.

6. D. R. Chakrabarty et al. Phys. Rev. **C36** (1987) 1886.

7. Aa. Bohr and B. Mottelson, Nuclear Structure vols. 1-2, 1969, Benjamin, New York.

8. D. M. Brink, in Proc. First Topical Meeting on Giant Resonance Excitation in Heavy Ion collisions, P.F. Bortignon, J. J. Gaardhøje, M. Di Toro (eds), Nucl. Phys. **A482** (1988).

9. B. L. Berman, Nuclear Data Tables **15** (1975) 321.

10. M. Gallardo et al., Nucl. Phys. **A443** (1985) 415.

11. S. Szymanski. Lecture at Masurian Lakes Summer School (1981), unpublished.

12. K. Neergaard, Phys. Lett. **B110** (1982) 7.

13. P. Ring in ref 5.

14. J. J. Gaardhøje. In: *Frontiers in Nuclear Dynamics*. Plenum Publishing Corporation (1985) 133-170.

15. M. Kicinska-Habior. Contribution to this conference.

16. K. A. Snover. Proc. Future Directions in Nuclear Spectroscopy, Strasbourg, AIP (1992).

17. Y. Alhassid et al., Phys. Rev. Lett. **57** (1986) 539.

18. Y. Alhassid et al., Phys. Rev. Lett. **65** (1990) 2527.

19. A. L. Goodman. Nucl. Phys. **A528** (1991) 348.

20. B. Lauritzen et al., Phys. Lett. **B207** (1988) 238.

21. Y. Alhassid et al., Phys. Rev. Lett **63** (1989) 2452.

22. E. Ormand et al., Phys. Rev. Lett. **64** (1990) 2254.

23. F. Camera et al., Phys. Lett. **B293** (1992) 18, and contribution to this conference.

24. A. Maj et al., Phys. Lett. **B291** (1992) 385, and contribution to this conference.

25. G. Enders et al., Phys. Rev. Lett. **69** (1992) 249.

26. K. Yoshida et al., Phys. Lett. **B245** (1990) 7.

27. A. Smerzi et al., Phys. Rev. **C44** (1991) 1713.

28. P. F. Bortignon et al., Phys. Rev. Lett. **67** (1991) 3360.